



# On the effective spectral emissivity of clear skies and the radiative cooling potential of selectively designed materials



Mengying Li, Carlos F.M. Coimbra\*

Department of Mechanical and Aerospace Engineering and Center for Energy Research, University of California San Diego, 9500 Gilman Drive, La Jolla, CA 92093, USA

## ARTICLE INFO

### Article history:

Received 24 October 2018

Received in revised form 11 February 2019

Accepted 12 February 2019

### Keywords:

Longwave atmospheric radiation

Spectral sky emissivity

Passive radiative cooling

## ABSTRACT

Thermophotonic devices are optically designed to be spectrally selective in order to reject heat to outer space through atmospheric windows of low thermal absorption. The determination of thermal equilibrium temperatures for thermophotonic devices requires the knowledge of the effective spectral emissivity of the sky. In this work, individual contributions of participating gases and aerosols to the spectral values of the sky emissivity are analyzed in the entire infrared spectrum as well as in seven distinct bands for which water vapor either dominates or is virtually transparent to infrared radiation. We also propose high-fidelity correlations for the effective sky emissivity as functions of the normalized ambient partial pressure of water vapor ( $p_w$ ) for both broadband and for the seven spectral bands. The correlations are derived using a combination of ground experimental data, high resolution spectral data for the main atmospheric constituents and spectral models to reconstruct the spectral distribution of infrared thermal radiation from the atmosphere to the ground. These results enable direct calculation of the equilibrium temperature and cooling efficiency of radiative cooling devices in terms of meteorological conditions observed at the surface level. For hot and dry conditions, the passive radiative coolers have a cooling potential of  $150.8 \text{ W m}^{-2}$  while for humid conditions, the coolers are mostly ineffective.

© 2019 Elsevier Ltd. All rights reserved.

## 1. Introduction

The balance between the absorbed and scattered shortwave solar radiation (wavelengths smaller than  $4 \mu\text{m}$ ) and the emitted, absorbed and scattered terrestrial longwave radiation (wavelengths greater than  $4 \mu\text{m}$ ) determines the temperature structure of the atmosphere and of the Earth's surface [1–3]. Surface downwelling longwave (DLW) radiation is essential for understanding atmospheric processes and climate change [4], but also for the thermal design of radiative cooling systems, cooling towers, solar power plants, and of the built environment in general [5–8].

Current interest in the optical designs of radiative cooling devices [9–13] that take advantage of atmospheric windows to reject heat to outer space requires detailed balance between the incoming thermal radiation from the sky (DLW) and the outgoing emissive power from the coolers in order to calculate the equilibrium temperatures and cooling efficiencies. These figures of merit (equilibrium temperatures and cooling efficiencies) depend on the local atmospheric conditions, which include the convective environment around the device and the downwelling radiative flux from the atmosphere. The convective contribution can be minimized by design, but the thermal radiation from the atmosphere

(the so-called “sky radiation”) is geometrically constrained by the ability of radiative cooling devices to radiate directly to outer space.

Absorption bands of water vapor dominate the absorption and emission of infrared radiation in the atmosphere when conditions are wet (high relative humidity). When the relative humidity is low, other contributors such as  $\text{CO}_2$  and aerosols contribute in a non-negligible way through specific bands of the spectrum to the overall thermal balance of the radiative cooling devices. Here we make extensive use of ground measurements, high-resolution spectral data for the main atmospheric constituents and a previously developed detailed spectral radiative model [14] in order to determine the effective emissivity of the sky for seven critical bands of the infrared spectrum. Thus, we present a complete spectral model that allows for determination of effective sky emissivities under clear skies that can, in turn, be used for a wide range of meteorological conditions.

## 2. The spectral radiative model

### 2.1. Model overview

In this section we describe a high-fidelity, spectrally resolved, plane-parallel, two-flux radiative model that is used to simulate

\* Corresponding author.

E-mail address: [ccoimbra@ucsd.edu](mailto:ccoimbra@ucsd.edu) (C.F.M. Coimbra).

the heat transfer through the various layers of the atmosphere. A more complete description of the model that includes a meticulous validation routine is available in [14]. Here we summarize concisely the main components of the model for the benefit of the reader.

A schematic of the plane parallel geometry is shown in Fig. 1. The atmosphere is divided into  $N$  non-uniform parallel layers according to a pressure ordinate system [14]. Standard AFGL mid-latitude summer profiles [15] for temperature and atmospheric gas concentrations are adopted with corrections for current surface atmospheric gas concentrations. Ozone concentrations at the ground surface are updated to 50 ppb [16], while concentrations of other gases remain at the values proposed in [14]. These corrections allow for different water vapor content (relative humidity) and for increasing concentrations of  $\text{CO}_2$  [14]. The most up-to-date HITRAN spectral data and MT\_CKD continuum model are used to calculate spectral and continuum absorption coefficients for all key participating gases [17,18]. The longwave spectral range from 0 to  $2500 \text{ cm}^{-1}$  is defined on a grid having a uniform resolution of  $0.01 \text{ cm}^{-1}$ . Approximations from Mie theory are used to model aerosol absorption and scattering coefficients. One of our previous works has shown that aerosol radiative forcing is mostly felt in the window band between 8 and  $14 \mu\text{m}$  [14]. For the modelled aerosols in the present work, the size parameter ( $x = 2\pi r/\lambda$ ) is greater than 0.2 in the 8–14  $\mu\text{m}$  band, so the Mie scattering formulation is appropriate [19]. The strongly forward scattering of aerosols is re-scaled and approximated by the  $\delta$ -M approach [20],

$$\hat{\kappa}_e = (1 - \tilde{\rho}_a e_g) \kappa_e, \quad \hat{\rho} = \frac{\tilde{\rho}(1 - e_g)}{1 - \tilde{\rho}_a e_g}, \quad (1)$$

where the extinction coefficient  $\kappa_e$  and single scattering albedo  $\tilde{\rho}$  are scaled using the asymmetry parameter  $e_g$ . More details on the comprehensive methods and specific submodels can be found in Ref. [14].

## 2.2. Energy balance between layers

The monochromatic attenuation of intensity along a path  $s$  for an isotropic scattering medium is (dependence on wavenumber  $\nu$  is omitted)

$$\frac{dl}{ds} = \kappa_e (1 - \hat{\rho}) I_b + \hat{\kappa}_e \hat{\rho} \bar{I} - \kappa_e I, \quad (2)$$

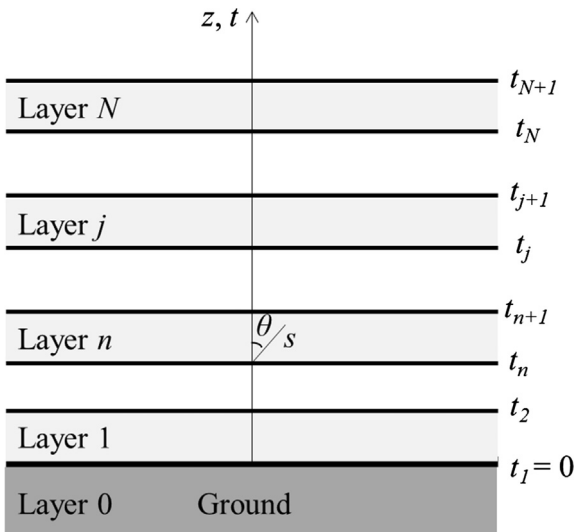


Fig. 1. Schematic of the plane parallel geometry.

where  $\hat{\kappa}_e \text{ (cm}^{-1}\text{)}$  is the extinction coefficient ( $\delta$ -M scaled),  $\hat{\rho}$  is the single scattering albedo ( $\delta$ -M scaled),  $I_b \text{ (W cm m}^{-2} \text{ sr}^{-1}\text{)}$  is the blackbody intensity in wavenumber basis according to Planck's law,  $I_b(\nu, T) = 2hc^2 \nu^3 / (\exp(\frac{hc}{k_b T \nu}) - 1)$ ,  $\bar{I}$  is the averaged intensity over all solid angles,  $\bar{I} = 1/4\pi \int_0^{4\pi} I d^2\omega$ . The radiosity  $J$  and irradiance  $G$  of a volume are

$$J = (1 - \hat{\rho}) \pi I_b + \hat{\rho} \pi \bar{I}, \quad G = \int_0^s e^{-t_{s'}} J(s') ds', \quad (3)$$

where the optical depth  $t_{s'} = \int_0^{s'} \hat{\kappa}_e(s'') ds''$ .

For a plane parallel layer of atmosphere as shown in Fig. 1, the irradiance is expressed using transfer factors [21]

$$G_n = \sum_j J_j \mathcal{F}_{nj} = \sum_j J_j \frac{1}{4\pi} \int_0^{4\pi} [e^{t_s - t_{sj}} - e^{t_s - t_{sj+1}}] d^2\omega, \quad (4)$$

where the transfer factor between layer  $n$  and layer  $j$  is defined as

$$\mathcal{F}_{nj} = \frac{1}{\Delta t_{s,n}} \int_{t_s} \int_0^{2\pi} d\phi \int_{\theta} [e^{t_s - t_{sj}} - e^{t_s - t_{sj+1}}] \frac{\sin \theta d\theta}{4\pi} dt_s. \quad (5)$$

Let  $u = 1/\cos \theta$ , then  $du = \sin \theta / \cos^2 \theta d\theta$  and  $\sin \theta d\theta = du/u^2$ . Note that the transfer factors given above can be written in terms of the normal optical depth  $t = \int_0^z \hat{\kappa}_e(z') dz'$ ,

$$\begin{aligned} \mathcal{F}_{nj} &= \frac{1}{2\Delta t_n} \int_t \int_1^\infty [e^{(t-t_j)u} - e^{(t-t_{j+1})u}] \frac{du}{u^2} dt \\ &= \frac{1}{2\Delta t_n} \int_{t_n}^{t_{n+1}} [E_2(t_j - t) - E_2(t_{j+1} - t)] dt \\ &= \frac{1}{2\Delta t_n} [E_3(|t_j - t_{n+1}|) + E_3(|t_{j+1} - t_n|) - E_3(|t_j - t_n|) \\ &\quad - E_3(|t_{j+1} - t_{n+1}|)], \end{aligned} \quad (6)$$

where  $E_2(\cdot)$  and  $E_3(\cdot)$  correspond to the second and third exponential integral functions defined by  $E_n(t) = \int_1^{+\infty} \exp(-ut)/u^n du$ , which integrate the intensity over all solid angles.

The transfer factor  $\mathcal{F}_{n,n}$  for a layer to itself (due to emission and scattering) is

$$\begin{aligned} \mathcal{F}_{n,n} &= 1 - \frac{1}{2\Delta t_n} \int_{t_n}^{t_{n+1}} [E_2(t_n - t) - E_2(t_{n+1} - t)] dt \\ &= 1 - \frac{1 - 2E_3(|t_{n+1} - t_n|)}{2(t_{n+1} - t_n)}. \end{aligned} \quad (7)$$

For each layer  $n$ , the radiosity  $J_n$  and irradiance  $G_n$  are then

$$G_n = \sum_{j=0}^{N+1} \mathcal{F}_{nj} J_j, \quad J_n = (1 - \tilde{\rho}_n) \pi \bar{I}_{b,n} + \tilde{\rho}_n G_n. \quad (8)$$

Note that the ground layer (layer 0) and outer space layer (layer  $N+1$ ) are included in the calculation because they contribute to the radiative energy balance. The optical depths of two boundaries are set to infinity, i.e.  $t_0 = -\infty$  and  $t_{N+2} = +\infty$ .

## 2.3. A plating algorithm for plane parallel geometries leads to modified transfer factors

The irradiation on each layer is a result of contributions of all layers, including the layer itself. To examine the spectral and vertical contribution to the irradiation on a particular layer  $n$ , a modified transfer factor  $\mathcal{F}_{nj}^*$  is defined to explicitly express monochromatic irradiation of layer  $n$  as

$$G_n = \sum_{j=0}^{N+1} \mathcal{F}_{nj}^* \pi \bar{I}_{b,j}. \quad (9)$$

The modified transfer factors  $\mathcal{F}_{n,j}^*$  are calculated from the transfer factors  $\mathcal{F}_{n,j}$  recursively using a plating algorithm [22]. Note that in Ref. [22], the plating algorithm was used for enclosures with grey surfaces but here the concept of recursive plating is adapted for scattering in volumetric atmospheric layers.

The plating algorithm for scattering is initiated by assuming all layers to be non-scattering, i.e., having albedo  $\hat{\rho} = 0$ ,

$$G_n = \sum_{j=0}^{N+1} \mathcal{F}_{n,j} \pi \bar{I}_{b,j}. \quad (10)$$

Then the algorithm applies a single scattering albedo  $\hat{\rho}$  value to one layer at a time recursively, starting from layer 0. Non-scattering layers are skipped. Upon the plating of layer  $k$ , the radiosity is converted from  $\pi \bar{I}_{b,k}$  to  $J_k$ , the sum of the emitted and scattered radiation,

$$J_k = \left(1 - \hat{\rho}_k\right) \pi \bar{I}_{b,k} + \hat{\rho}_k G_k^*, \quad \text{and} \quad G_k^* = \sum_{j \neq k} \mathcal{F}_{k,j} \pi \bar{I}_{b,j} + \mathcal{F}_{k,k} J_k, \quad (11)$$

where \* denotes the corrected irradiance value after plating.

Combining the relations in (11) gives the radiosity

$$J_k = \frac{1 - \hat{\rho}_k}{D_k} \pi \bar{I}_{b,k} + \frac{\hat{\rho}_k}{D_k} \sum_{j \neq k} \mathcal{F}_{k,j} \pi \bar{I}_{b,j}, \quad (12)$$

where the denominator is  $D_k = 1 - \hat{\rho}_k \mathcal{F}_{k,k}$ .

When  $i$  is different from  $k$ , the new value of irradiance after plating layer  $k$  is given by

$$\begin{aligned} G_i^* &= \sum_{j \neq k} \mathcal{F}_{i,j} \pi \bar{I}_{b,j} + \mathcal{F}_{i,k} J_k \\ &= \sum_{j \neq k} \left[ \mathcal{F}_{i,j} + \frac{\hat{\rho}_k}{D_k} \mathcal{F}_{i,k} \mathcal{F}_{k,j} \right] \pi \bar{I}_{b,j} + \frac{1 - \hat{\rho}_k}{D_k} \mathcal{F}_{i,k} \pi \bar{I}_{b,k}. \end{aligned} \quad (13)$$

The irradiance of layer  $k$  itself is then affected by the single scattering albedo,

$$\begin{aligned} G_k^* &= \left(1 - \hat{\rho}_k\right) \sum_{j \neq k} \mathcal{F}_{k,j} \pi \bar{I}_{b,j} + \left(1 - \hat{\rho}_k\right) \mathcal{F}_{k,k} J_k \\ &= \left(1 - \hat{\rho}_k\right) \sum_{j \neq k} \left[ \mathcal{F}_{k,j} + \frac{\hat{\rho}_k}{D_k} \mathcal{F}_{k,k} \mathcal{F}_{k,j} \right] \pi \bar{I}_{b,j} \\ &\quad + \frac{\left(1 - \hat{\rho}_k\right)^2}{D_k} \mathcal{F}_{k,k} \pi \bar{I}_{b,k}. \end{aligned} \quad (14)$$

Comparison of Eqs. (13) and (14) with Eq. (9) reveals the existence of four cases:

$$\begin{cases} \mathcal{F}_{i,j}^* = \mathcal{F}_{i,j} + \frac{\hat{\rho}_k}{D_k} \mathcal{F}_{i,k} \mathcal{F}_{k,j}, & i \neq k, j \neq k, \\ \mathcal{F}_{i,k}^* = \frac{1 - \hat{\rho}_k}{D_k} \mathcal{F}_{i,k}, & i \neq k, j = k, \\ \mathcal{F}_{k,j}^* = \left(1 - \hat{\rho}_k\right) \left[ \mathcal{F}_{k,j} + \frac{\hat{\rho}_k}{D_k} \mathcal{F}_{k,k} \mathcal{F}_{k,j} \right] = \frac{1 - \hat{\rho}_k}{D_k} \mathcal{F}_{k,j}, & i = k, j \neq k, \\ \mathcal{F}_{k,k}^* = \frac{\left(1 - \hat{\rho}_k\right)^2}{D_k} \mathcal{F}_{k,k}, & i = k, j = k. \end{cases} \quad (15)$$

After plating, the modified transfer factors satisfy  $\sum_{j=0}^{N+1} \mathcal{F}_{k,j}^* = 1 - \hat{\rho}_k$ .

#### 2.4. The effective emissivity of the sky

Once the modified transfer factors are obtained, the energy transfer between each layer can be explicitly calculated using Eq. (9). After solving for the downwelling spectral flux density  $G_0(v)$

at the ground surface, the radiosity of the sky and the effective sky emissivity are defined as

$$\begin{aligned} J_{\text{sky}} &= \int_0^{+\infty} G_0(v) dv, \\ \varepsilon_{\text{sky}} &= \frac{J_{\text{sky}}}{\sigma T_a^4}, \end{aligned} \quad (16)$$

where  $v$  is the wavenumber ( $\text{cm}^{-1}$ ),  $\sigma = 5.67 \times 10^{-8} \text{ W m}^{-2} \text{ K}^{-4}$  is the Stefan-Boltzmann constant and  $T_a$  (K) is the air temperature at the screening level (10 m above the surface).

### 3. Contributors to the effective spectral emissivity for clear skies

Brunt (1932) has shown that the broadband sky emissivity is strongly correlated to the concentration of water vapor and temperature at the screening (ground) level [23]. The strong correlation results from two different-yet-related mechanisms: (i) a value of the broadband sky emissivity that is dominated by contributions from the lowest layers of the atmosphere, especially during humid ambient conditions, and (ii) thermal absorption of the infrared spectrum that is dominated by the wide absorption bands of water vapor. The following sections utilize the radiative model presented above (Section 2) to empirically verify the existence of the two mechanisms.

#### 3.1. Broadband contributions from different atmospheric layers

With the use of modified transfer factors and Eq. (9), the broadband contributions of irradiance flux of each layer from all other layers can be analyzed, as shown in Fig. 2, for an atmosphere with surface relative humidity of 65% and aerosol optical depth at 479.5 nm equal to 0.1. The summation of each row in Fig. 2(a) is equal to total irradiance to the layer and the summation of each row in Fig. 2(b) is equal to 100%. The  $x$ -axis represents irradiance origin layer  $j$  in Eq. (9) while the  $y$ -axis represents irradiance destination layer  $n$  in Eq. (9). As shown in Fig. 2, 65.3% of longwave irradiation to the ground surface comes from the nearest atmospheric layer, 15.3% comes from the second nearest layer, 7.4% comes from the third nearest layer and the remainder 12.0% comes from all other layers. For the nearest atmospheric layer, 27.7% of its longwave irradiation comes from the surface, 52.5% comes from itself, 11.2% comes from the layer above it and the rest 8.6% comes from all other layers. Similarly, 18.4% of the second nearest atmospheric layer longwave irradiation comes from the surface, 4.3% comes from the layer below it, 63.1% comes from itself, 8.0% comes from the layer above it, while the remainder 6.2% comes from other layers. From the nearest atmosphere layer to the tropopause layer (layer 13), the largest contribution to the irradiation on the layer is from the layer itself. Above the tropopause, the largest contribution is from the ground layer. The layers above the tropopause contribute less than 4.8% to the irradiance to other layers due to lower temperature levels.

Thus, our model empirically demonstrates that the value of the broadband sky emissivity is dominated by contributions from the lowest layers of the atmosphere.

#### 3.2. Broadband contributions from atmospheric constituents

We consider the broadband contribution of  $\text{H}_2\text{O}$  to  $\varepsilon_{\text{sky}}$  when only  $\text{H}_2\text{O}$  is participating (because  $\text{H}_2\text{O}$  is the main constituent responsible for the vertical temperature profile in the troposphere). Contributions of other atmospheric constituents are obtained by calculating the difference of  $\varepsilon_{\text{sky}}$  when the respective constituent were absent. Therefore, the net contribution (devoid of band overlaps) of constituent  $i$  to  $\varepsilon_{\text{sky}}$  is calculated as

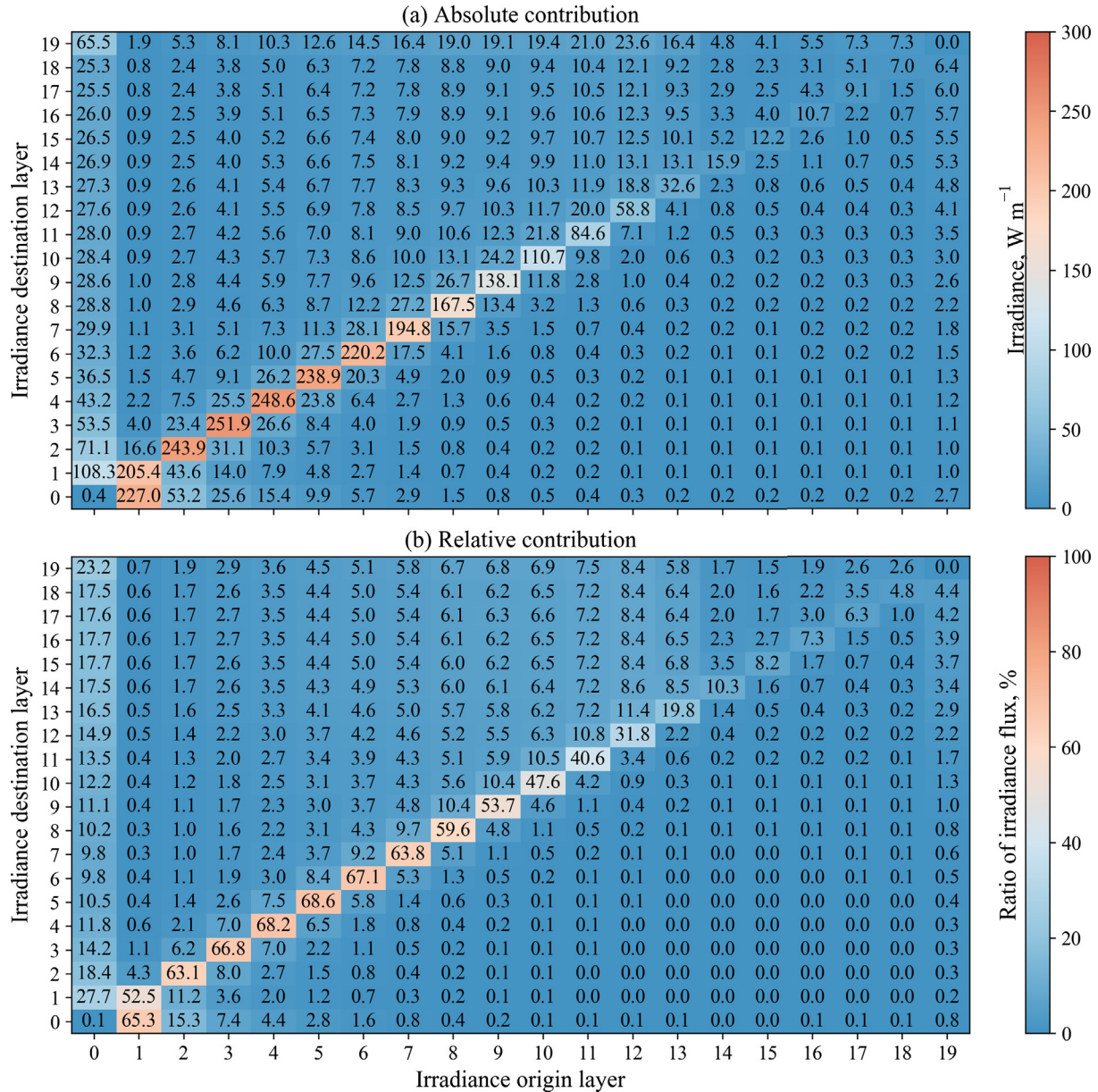


Fig. 2. Broadband (a) absolute contributions and (b) relative contribution of irradiance flux of each layer. Ground condition is  $\phi = 65\%$  and AOD = 0.1.

$$\varepsilon_{\text{sky},i} = \frac{J_{\text{sky}}(w_i)}{\sigma T_a^4} \quad \text{for } i = \text{H}_2\text{O}, \quad (17)$$

$$\varepsilon_{\text{sky},i} = \frac{J_{\text{sky}}(\sum_k w_k) - J_{\text{sky}}(\sum_{k \neq i} w_k)}{\sigma T_a^4} \quad \text{for } i \neq \text{H}_2\text{O},$$

where  $w_i$  represents the volumetric mixing ratio of constituent  $i$ . Since the band overlaps have been extracted more than once when calculating  $J_{\text{sky}}(\sum_{k \neq i} w_k)$ , so an  $\varepsilon_{\text{sky,overlap}}$  term is added to account for the total band overlaps. Then the total  $\varepsilon_{\text{sky}}$  is expressed as

$$\varepsilon_{\text{sky}} = \sum_i \varepsilon_{\text{sky},i} + \varepsilon_{\text{sky,overlap}}. \quad (18)$$

The relative contribution of each constituent and overlap is then

$$r_i = \frac{\varepsilon_{\text{sky},i}}{\varepsilon_{\text{sky}}}. \quad (19)$$

The absolute and relative contributions of atmospheric constituents are plotted in Fig. 3 with respect to normalized partial pressure of water vapor  $p_w$  at the screening level ( $p_w = P_w/P_0$  where  $P_0 = 1.013 \times 10^5$  Pa). The absolute and relative contribu-

tions of  $\text{H}_2\text{O}$  increase with  $p_w$  while those of other constituents decrease with  $p_w$ . When sufficient  $\text{H}_2\text{O}$  is present in the atmosphere, a large portion of the infrared spectrum is saturated by water vapor, leaving other constituents' contributions negligible. Water vapor contributes from 71.2% (dry conditions) to 97.3% (humid conditions) of the broadband effective sky emissivity, while  $\text{CO}_2$  contributes from 17.9% to 0.7%. The contribution of  $\text{O}_3$  ranges from 1.9% to 0.7%. The contributions of aerosols range from 2.5% to 0.5% and those of  $\text{N}_2\text{O}$  and  $\text{CH}_4$  range from approximately 0.9% to 0.02%, while oxygen and nitrogen contribute a negligible amount.

The contributions of each constituent and overlaps to the broadband effective sky emissivity are fitted using a power law expression

$$\varepsilon_{\text{sky},i} = c_{1,i} + c_{2,i}(p_w)^{c_{3,i}}, \quad (20)$$

where  $c_{1,i}$ ,  $c_{2,i}$  and  $c_{3,i}$  are obtained from least-squares regression of the available data. These are presented in Table 1. Note that since the empirical expression regressed in Ref. [8] uses water vapor

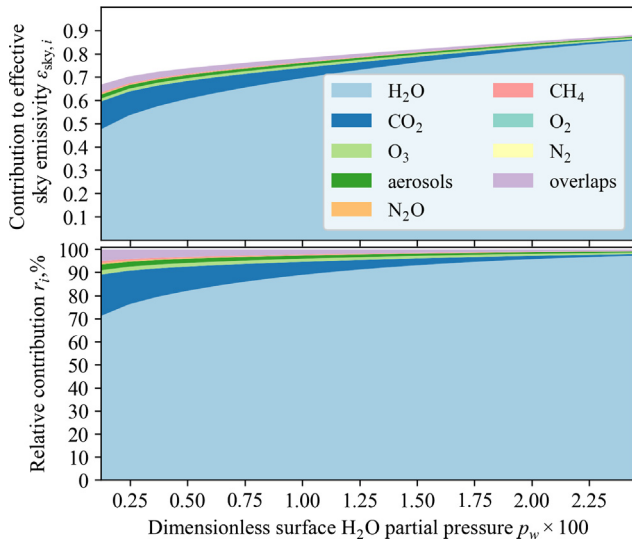


**Fig. 3.** Broadband contribution of each atmospheric constituent to effective sky emissivity. Upper and lower subplots show absolute and relative contributions, respectively.

partial pressure  $p_w$  in hPa as the independent variable instead of dimensionless  $p_w$ , the coefficient  $c_{2,E}$  ('E' stands for empirical) has been modified accordingly. For the contribution of each constituent, the values of  $c_{2,i}$  are negative for constituents other than H<sub>2</sub>O because their contributions decrease with increasing water vapor concentration. The  $c_{2,i}$  is nearly zero for CH<sub>4</sub> indicating that the contribution of CH<sub>4</sub> is weakly dependent on the amount of H<sub>2</sub>O, because their absorbing bands are not overlapped. The contribution of water vapor alone increases with  $(p_w)^{0.3784}$ . When all constituents are added, the value of  $c_{3,T}$  ('T' stands for total) increases to 0.5035, which is close to the empirical model proposed in [8].

### 3.3. Spectral band contributions from each atmospheric constituent

To further analyze the spectral contribution of each atmospheric constituent, the longwave spectrum is divided into seven bands: four absorbing bands and three window (non-absorbing) bands. The two absorbing bands of water vapor are (b1) 0–400 cm<sup>-1</sup> and (b5) 1400–2250 cm<sup>-1</sup>. The two absorbing bands of CO<sub>2</sub> are (b3) 580–750 cm<sup>-1</sup> and (b6) 2250–2400 cm<sup>-1</sup>. The three window bands (b2), (b4) and (b7) are in between the absorbing bands. The division of bands with the spectral extinction coefficient of each constituent are plotted in Fig. 4, where the absorbing bands of water vapor and CO<sub>2</sub> are readily identified. The band boundaries are defined so that bands (b1), (b2), (b5), and (b7) have contributions from water vapor alone, while the contribution of CO<sub>2</sub> is only prominent in (b3), (b4), and (b6).

The contributions in band  $j$  from atmospheric constituent  $i$  are defined as

$$\epsilon_{sky,ij} = \epsilon_{sky,i}(\Delta v_j), \quad (21)$$

where  $\Delta v_j$  represents the wavenumber range of band  $j$ .

In Fig. 5, we have plotted the contributions in each band from each atmospheric constituent with respect to  $p_w$ . The contributions from bands (b6) and (b7) are small because little longwave would be emitted in those wavenumbers according to Planck's law. A small amount of water vapor saturates bands (b1) and (b5) so that the contribution of water vapor does not increase with  $p_w$  and the contributions from other constituents are nearly zero in these two bands. For band (b2), the contribution of water vapor increases with increased  $p_w$  then becomes saturated when  $p_w > 0.01$ , and the contributions from other constituents are negligible. Water vapor, CO<sub>2</sub> and overlap saturate band (b3), so that the total contribution of the three is nearly invariant with  $p_w$ . Since (b3) is an absorbing band of CO<sub>2</sub>, it defines the spectral region where the contribution of CO<sub>2</sub> is most significant. If the atmosphere had no CO<sub>2</sub> (assume all CO<sub>2</sub> is harvested from the atmosphere), band (b3) would become unsaturated even for very humid conditions, making (b3) another window band for radiative cooling. The contributions of O<sub>3</sub>, N<sub>2</sub>O, CH<sub>4</sub> and aerosols are only relevant in band (b4), the so-called 'atmospheric window'. As expected, the contribution of water vapor increases with increased values of  $p_w$  while the relative contributions from other constituents decrease. Note that band (b4) is unsaturated even for very humid conditions, leaving it the spectral window for radiative cooling.

The contributions from each constituent in each band to the broadband effective sky emissivity are fitted using Eq. (20) and the coefficients of  $c_1$ ,  $c_2$  and  $c_3$  are tabulated in Table 2. Since band (b2) shows a non-power law asymptotic behavior, a hyperbolic function is used as the fitting function instead. With these tabulated values, each individual contribution to the different atmospheric bands can be easily calculated for any value of ambient  $p_w$ .

Furthermore, Fig. 6 presents the relative contribution in each band from each constituent  $r_{ij}$ :

$$r_{ij} = \frac{\epsilon_{sky,ij}}{\epsilon_{sky,j}}, \quad (22)$$

where  $\epsilon_{sky,ij}$  is the contribution in band  $j$  from atmospheric constituent  $i$  and  $\epsilon_{sky,j}$  is the contribution in band  $j$  from all constituents. In bands (b1), (b2) and (b5), water vapor is the only contributor regardless of ambient  $p_w$ , so its relative contribution is 100%. The relative contribution of CO<sub>2</sub> ranges from 64.4% to 3.3% in band (b3) and ranges from 11.2% to 1.1% in band (b4). There is a strong absorbing band of O<sub>3</sub> in band (b4) where O<sub>3</sub> contributes to 11.0% to 2.3%. For bands (b6) and (b7), with the presence of CO<sub>2</sub>, the band emissivity reduces thus resulting in a negative contribution.

Fig. 7 presents the relative contribution by band from each constituent to the total effective sky emissivity with respect to the ambient  $p_w$ :

$$r_{ij} = \frac{\epsilon_{sky,ij}}{\epsilon_{sky}}, \quad (23)$$

where  $\epsilon_{sky}$  is the total effective sky emissivity. The summation of relative contribution from all bands for a particular  $p_w$  equals to 100%. Band (b1) contributes 25.6% to 19.6% to the total sky emissivity and the contribution decreases as increased ambient  $p_w$ . Band (b2) contributes to 23.6% to 20.5% while the contribution first increases then decreases with increased ambient  $p_w$ . Band (b3) contributes to 25.0% to 19.8% and the contribution of water vapor

**Table 1**  
Regression coefficients for the contribution of each constituent to the broadband effective sky emissivity given by Eq. (20).

	H <sub>2</sub> O	CO <sub>2</sub>	O <sub>3</sub>	Aerosols	N <sub>2</sub> O	CH <sub>4</sub>	O <sub>2</sub>	N <sub>2</sub>	Overlaps	Total	Ref. [8]
$c_1$	0.2996	0.2893	0.0126	0.0191	13.8712	0.0245	–	–	0.0524	0.6173	0.5980
$c_2$	2.2747	–0.5640	–0.5119	–0.1421	–13.8761	–0.0313	–	–	–0.1423	1.6940	1.8140
$c_3$	0.3784	0.1821	1.1744	0.6121	0.0001	0.0790	–	–	0.2998	0.5035	0.5000
R <sup>2</sup>	0.9998	0.9959	0.9997	0.9992	0.9990	1.0000	–	–	0.9997	0.9978	

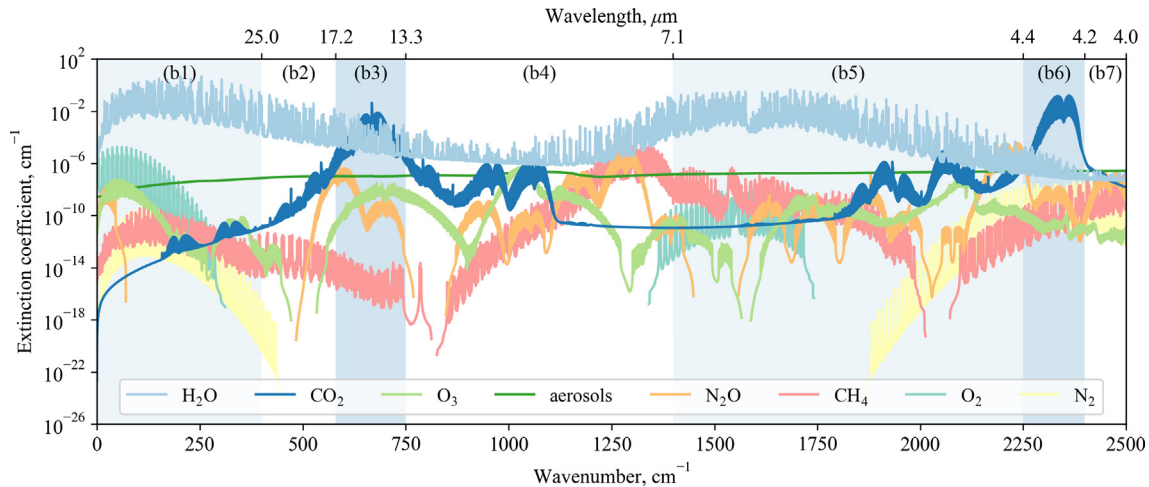


**Fig. 4.** Spectral extinction coefficients for the main atmospheric constituents at the lowest layer of the troposphere. The spectral line absorption coefficients of gases are obtained from HITRAN database while continuum absorption coefficients are calculated by the MT\_CKD continuum model. The extinction coefficients of aerosols are calculated by Mie theory. Colored shades indicate the absorbing bands of water vapor (lighter) and CO<sub>2</sub> (darker). The interested reader is directed to Ref. [14] for greater detail.

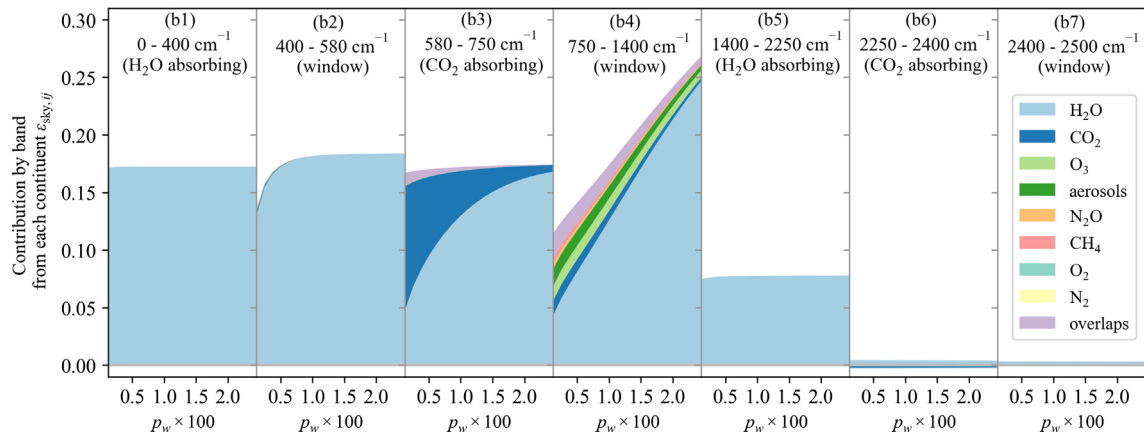


**Fig. 5.** Contributions to the effective sky emissivity by atmospheric wavenumber band from each atmospheric constituent.

increases with increased  $p_w$  while the contributions of CO<sub>2</sub> and overlap decreases with increased  $p_w$ . The contribution of band (b4) increases near linearly from 17.1% to 30.5% with respect to ambient  $p_w$ . Water vapor in band (b5) contributes to approximately 10%. The contributions from bands (b6) and (b7) are smaller than 0.5%.

#### 4. Cooling potential of passive radiative coolers under clear skies

##### 4.1. The broadband cooling power

Passive radiative coolers are designed to have low absorptance in the solar shortwave spectrum and high emittance in the infrared longwave spectrum [10,12], so that they can reject heat through the ‘atmospheric window’ (denoted as band (b4) in this work) even under direct sunlight. With the correlations for spectral atmospheric emissivity, it is possible to estimate the cooling power of different materials used for passive cooling that take advantage of the atmospheric window. The broadband net cooling power  $q_{\text{cool}}(T)$  of a radiative cooler of surface temperature  $T$  is [10]

$$q_{\text{cool}}(T) = \bar{\epsilon}_{lw} \left[ \sigma T^4 - J_{\text{sky}}(T_a, \phi) \right] - \bar{\epsilon}_{sw} q_{\text{sun}} - h_c (T_a - T), \quad (24)$$

where  $\bar{\epsilon}_{lw}$  (or  $\bar{\epsilon}_{sw}$ ) are the spectral averaged longwave (or shortwave) emittance/absorptance of the cooler,  $J_{\text{sky}}(T_a, \phi)$  ( $\text{W m}^{-2}$ ) is the sky radiation calculated using the methods proposed in Section 3,  $q_{\text{sun}}$  ( $\text{W m}^{-2}$ ) is the shortwave solar irradiance,  $h_c$  ( $\text{W m}^{-2} \text{K}^{-1}$ ) is the convective heat transfer coefficient and  $T_a$  (K) is the ambient temperature.

When  $T = T_a$ ,  $q_{\text{cool}}(T = T_a)$  defines the cooling power at the ambient temperature [10]

$$q_{\text{cool}}(T_a) = \bar{\epsilon}_{lw} \sigma T_a^4 [1 - \epsilon_{\text{sky}}(T_a, \phi)] - \bar{\epsilon}_{sw} q_{\text{sun}}, \quad (25)$$

where the broadband cooling power decreases with increased effective sky emissivity.

The cooling power  $q_{\text{cool}}(T_a)$  of the photonic material described in [12] for different ambient meteorological conditions is shown in Fig. 8. This material in particular has an averaged solar absorptance of 0.04 and longwave absorptance/emittance of 0.93 [12]. For the purposes of calculation, the daytime solar irradiance is set to  $890 \text{ W m}^{-2}$  [10], and the broadband sky emissivity is calculated using Eq. (20) with coefficients tabulated in Table 2. Fig. 8 shows the cooling power during daytime periods. The nighttime cooling power for the same conditions is  $0.04 \times 890 = 35.6 \text{ W m}^{-2}$  more, because of zero absorption of solar irradiance during the night. The cooling power is high for hot and dry conditions, and

**Table 2**  
Fitting coefficients for contributions from each constituent in each band to the total effective sky emissivity.

		H <sub>2</sub> O	CO <sub>2</sub>	O <sub>3</sub>	Aerosols	N <sub>2</sub> O	CH <sub>4</sub>	O <sub>2</sub>	N <sub>2</sub>	Overlaps	Total
Band (b1)	c <sub>1</sub>	0.1725	-	-	-	-	-	-	-	-	0.1725
	c <sub>2</sub>	-	-	-	-	-	-	-	-	-	-
	c <sub>3</sub>	-	-	-	-	-	-	-	-	-	-
	R <sup>2</sup>	-	-	-	-	-	-	-	-	-	-
Band (b2)*	c <sub>1</sub>	0.1083	0.0002	-	0.0002	0.0001	-	-	-	0.0003	0.1170
	c <sub>2</sub>	0.0748	-	-	-	-	-	-	-	-	0.0662
	c <sub>3</sub>	270.8944	-	-	-	-	-	-	-	-	270.4686
	R <sup>2</sup>	0.9927	-	-	-	-	-	-	-	-	0.9926
Band (b3)	c <sub>1</sub>	-0.2308	0.3038	-	0.0001	0.0001	-	-	-	17.0770	0.1457
	c <sub>2</sub>	0.6484	-0.5262	-	-	-	-	-	-	-17.0907	0.0417
	c <sub>3</sub>	0.1280	0.1497	-	-	-	-	-	-	0.0002	0.0992
	R <sup>2</sup>	0.9953	0.9950	-	-	-	-	-	-	0.9946	0.9985
Band (b4)	c <sub>1</sub>	0.0289	0.0144	0.0129	0.0159	0.0018	0.0243	-	-	0.0227	0.1057
	c <sub>2</sub>	6.2436	-0.1740	-0.4970	-0.3040	-	-0.0312	-	-	-0.2748	5.8689
	c <sub>3</sub>	0.9010	0.7268	1.1620	0.8828	-	0.0795	-	-	0.7480	0.9633
	R <sup>2</sup>	0.9998	0.9979	0.9997	0.9989	-	1.0000	-	-	0.9993	0.9998
Band (b5)	c <sub>1</sub>	0.0775	-	-0.0002	-	-0.0006	-	-	-	-0.0001	0.0766
	c <sub>2</sub>	-	-	-	-	-	-	-	-	-	-
	c <sub>3</sub>	-	-	-	-	-	-	-	-	-	-
	R <sup>2</sup>	-	-	-	-	-	-	-	-	-	-
Band (b6)	c <sub>1</sub>	0.0044	-0.0022	-	-	-	-	-	-	-0.0002	0.0019
	c <sub>2</sub>	-	-	-	-	-	-	-	-	-	-
	c <sub>3</sub>	-	-	-	-	-	-	-	-	-	-
	R <sup>2</sup>	-	-	-	-	-	-	-	-	-	-
Band (b7)	c <sub>1</sub>	0.0033	-0.0003	-	-0.0001	-0.0001	-	-	-	-0.0002	0.0026
	c <sub>2</sub>	-	-	-	-	-	-	-	-	-	-
	c <sub>3</sub>	-	-	-	-	-	-	-	-	-	-
	R <sup>2</sup>	-	-	-	-	-	-	-	-	-	-

Note\*: For band (b2), the fitting function has the form of a hyperbolic tangent function  $\epsilon_{sky,i} = c_{1,i} + c_{2,i} \tanh(c_{3,i} p_w)$ .

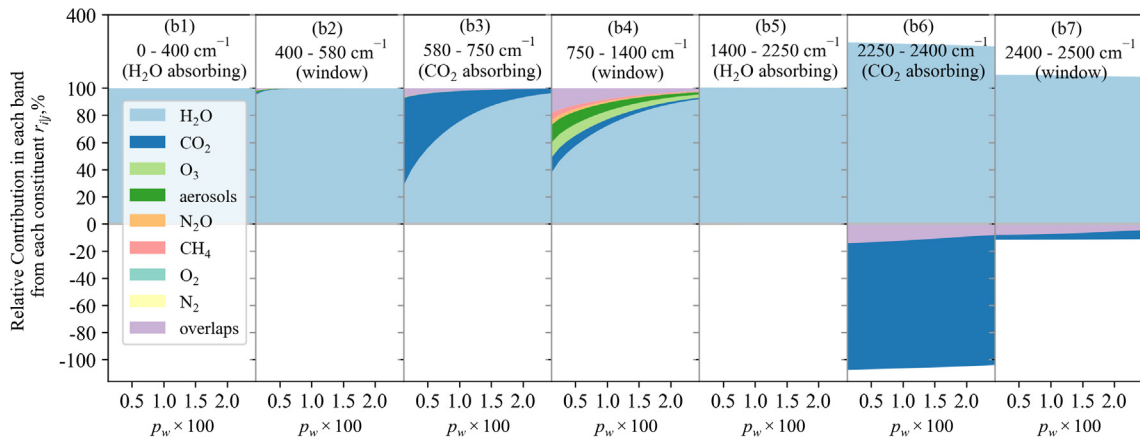


**Fig. 6.** Relative contribution from each atmospheric constituent to each band with respect to  $p_w$ .

substantially lower for mild temperatures and high humidities. Ref. [12] reports cooling rate ranges from 100 to 145 W m<sup>-2</sup>, which falls within the conditions plotted in Fig. 8.

In the absence of net power outflow, the temperature of radiative coolers should reach a steady state value  $T_s$  [10] and this temperature needs to be below  $T_a$  to enable cooling. At steady state, the thermo-derivative vanishes and the surface temperature is solved by equating:

$$\bar{\epsilon}_{lw} [\sigma T_s^4 - J_{sky}(T_a, \phi)] = \bar{\epsilon}_{sw} q_{sun} + h_c (T_a - T_s). \quad (26)$$

For the passive cooling material proposed in [12], the steady state temperature  $T_s$  is then calculated for different ambient temperatures  $T_a$  and relative humidities  $\phi$ . The convective heat transfer coefficient is taken to be  $h_c = 6.9$  W/m K [10]. Fig. 9 plots the

temperature difference ( $T_a - T_s$ ) for four scenarios: daytime with or without convection and nighttime with or without convection. The temperature difference ( $T_a - T_s$ ) decreases with increased  $p_w(T_a, \phi)$  because of increased effective sky emissivity due to higher water vapor concentration in the atmosphere. Both the convective heat gain from ambient air and the absorption of solar radiation reduce ( $T_a - T_s$ ), which in turn reduce the cooling potential of the radiative coolers.

#### 4.2. The spectral cooling power

The spectral longwave cooling power at ambient temperature  $q_{cool,lw}(v, T_a)$  is

$$q_{cool,lw}(v, T_a) = \epsilon_{lw}(v) \pi I_b(T_a, v) [1 - \epsilon_{sky}(v, T_a, \phi)]. \quad (27)$$

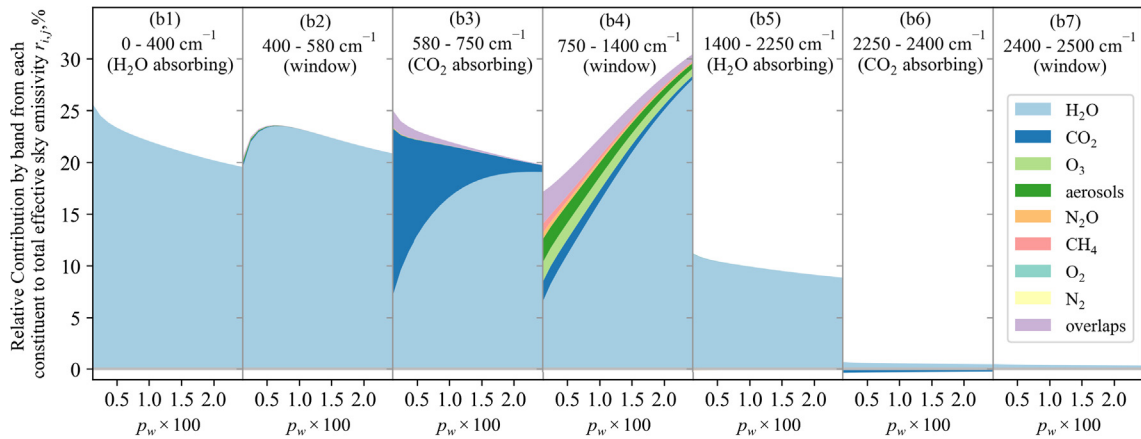


Fig. 7. Relative contribution by band from each atmospheric constituent to total effective sky emissivity with respect to  $p_w$ .

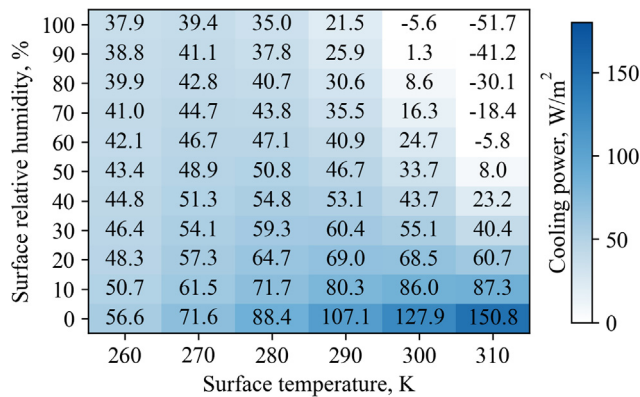


Fig. 8. Cooling power potential of a passive cooling material under different ambient meteorological conditions during daytime when  $q_{\text{sun}} = 890 \text{ W/m}^2$ .

Fig. 10 plots the spectral emitted longwave radiation and cooling power of the material under clear skies when  $T_a = 294.2 \text{ K}$ . The cooling is mostly in bands (b2) and (b4) and decreases with increased ambient relative humidity (representative of atmospheric column water vapor concentration).

Since only bands (b2) and (b4) contribute to the cooling power, by applying the regressed coefficients for bands (b2) and (b4) tabulated in Table 2 the cooling power per band is plotted in Fig. 11(b) for ambient  $T_a = 294.2 \text{ K}$ . The longwave cooling power is mostly from band (b4) and it decreases with increased ambient relative humidity (proportional to the column of water vapor content in the atmosphere) because atmospheric  $\text{H}_2\text{O}$  ‘blocks’ the atmospheric window. Fig. 11(a) is a plot of the cooling power by band calculated by line-by-line integration of the spectral cooling power in each band. The difference in values between Fig. 11(a) and (b) is less than 6%, indicating that the coefficients proposed in Table 2 can be used to estimate sky emissivity in each band with sufficient accuracy for thermal design applications.

### 5. Conclusions

A detailed spectral model of the main atmospheric constituents is used to correlate longwave band emissivities for the downwelling longwave radiation from the Earth’s atmosphere. Modified transfer factors are found recursively through a plating algorithm. The results show that for a cloud-free atmosphere with screening

level relative humidity of 65%, about 65.3% of the downwelling longwave radiation comes from the lowest atmospheric layer. In addition, the column of water vapor contributes between 71.2% (dry conditions) and 97.3% (wet conditions) of the total radiating flux. Therefore, the water vapor concentration in the lowest atmospheric layer correlates very well with the effective emissivity of clear skies.

The infrared (longwave) spectrum is divided into seven distinct bands, in which two of them have negligible contributions because of their small blackbody emissive power. In three out of the five contributor spectral bands, water vapor is the sole contributor to the emissivity of the sky, and the contribution is weakly dependent on water vapor content. This indicates that a small concentration of water vapor is enough to saturate these bands. The contribution from  $\text{CO}_2$  is most obvious in its absorbing band (b3) from 580 to  $750 \text{ cm}^{-1}$ , in which  $\text{H}_2\text{O}$  and  $\text{CO}_2$  together saturate the band. When the band is saturated, emissivities are mostly independent of water vapor content. If  $\text{CO}_2$  molecules were absent from the atmosphere, water vapor alone would not have the potential to saturate band (b3), so that this band would be another important spectral window for radiative cooling. Only in the atmospheric window band (b4) do contributions from other atmospheric constituents like  $\text{O}_3$ , aerosols,  $\text{N}_2\text{O}$  and  $\text{CH}_4$  become non-negligible. The emissivity of band (b4) increases approximately as a linear function of water vapor concentration and is not saturated even under conditions of high humidity. The b4 band is the main spectral window for radiative cooling.

The band emissivities are then correlated by simple expressions to ambient meteorological conditions at the ground level (temperature and relative humidity), which allow for the expedient calculation of cooling power efficiencies for any optically selective material designed for passive radiative cooling. These simple expressions also allow for the determination of equilibrium temperatures and thermal fluxes for agricultural, meteorological and climatological applications. Comparisons between band calculations and line-by-line calculations yield errors that are generally within the measurement uncertainty of atmospheric instrumentation (e.g., pyrgeometers or broadband pyranometers, with uncertainties ranging from 3 to 6%). These small deviations validate the combined approach of high fidelity spectral models with ground experiments taken at diverse micro-climates, altitudes and meteorological conditions.

For hot and dry ambient conditions, radiative cooling power potentials are as high as  $150.8 \text{ W m}^{-2}$  while for humid conditions, the cooling power potential decreases substantially. For hot and wet conditions, radiative coolers are mostly ineffective.

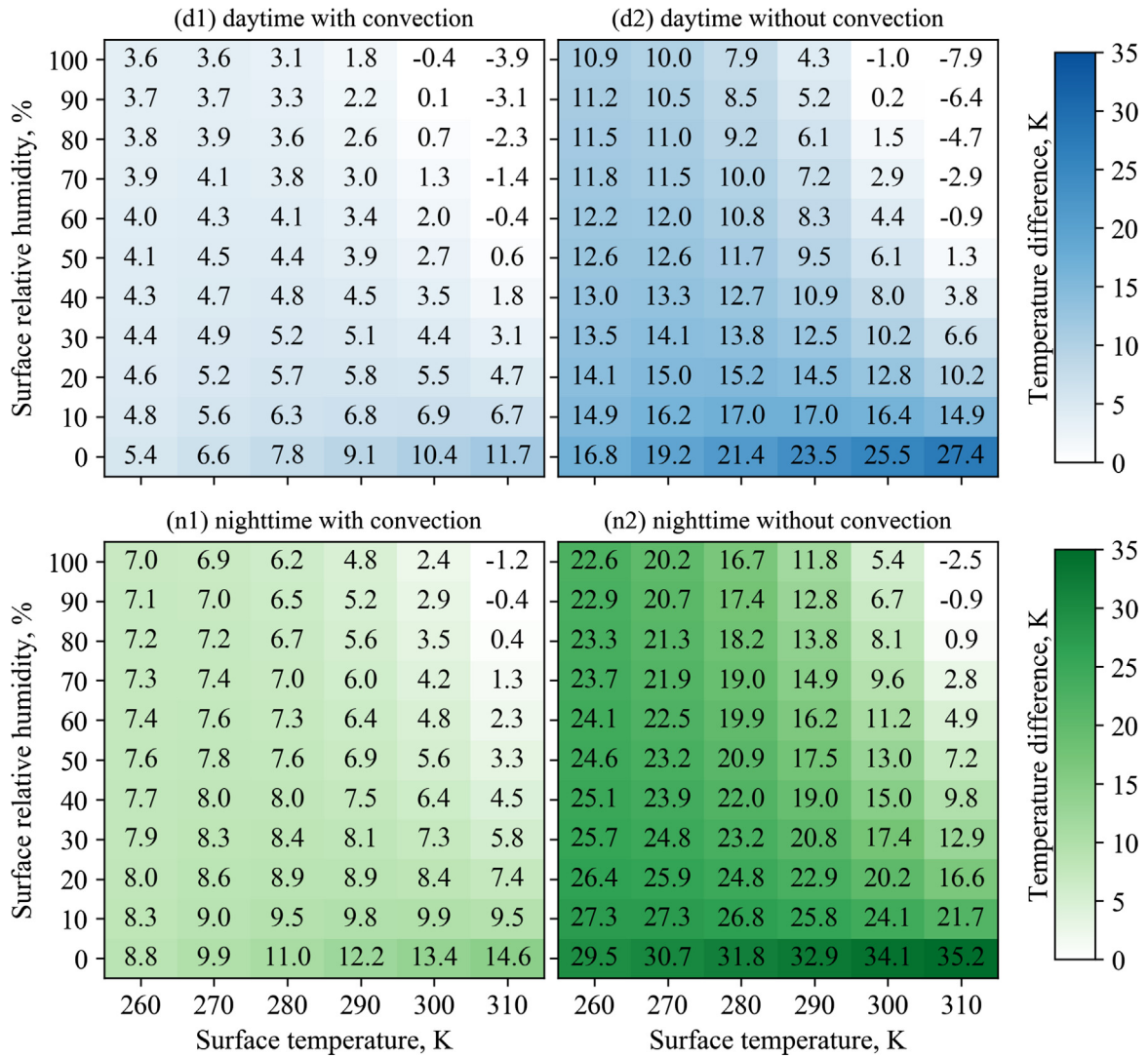


**Fig. 9.** Temperature difference ( $T_a - T_s$ ) of the passive cooling material under different ambient meteorological conditions. (d1) is for daytime when  $q_{\text{sun}} = 890 \text{ W m}^{-2}$  and  $h_c = 6.9 \text{ W m}^{-2} \text{ K}^{-1}$ . (d2) is for daytime when  $q_{\text{sun}} = 890 \text{ W m}^{-2}$  and  $h_c = 0$ . (n1) is for nighttime when  $q_{\text{sun}} = 0$  and  $h_c = 6.9 \text{ W m}^{-2} \text{ K}^{-1}$ . (n2) is for nighttime when  $q_{\text{sun}} = 0$  and  $h_c = 0$ .

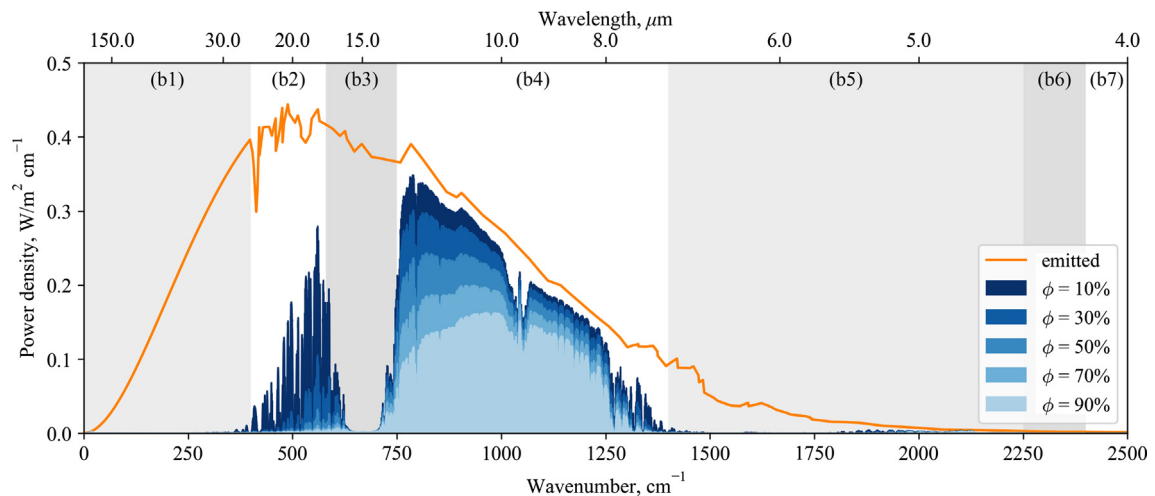


**Fig. 10.** Spectral longwave cooling power  $q_{\text{cool,lw}}(\nu, T_a)$  for ambient  $T_a = 294.2 \text{ K}$  under clear skies.

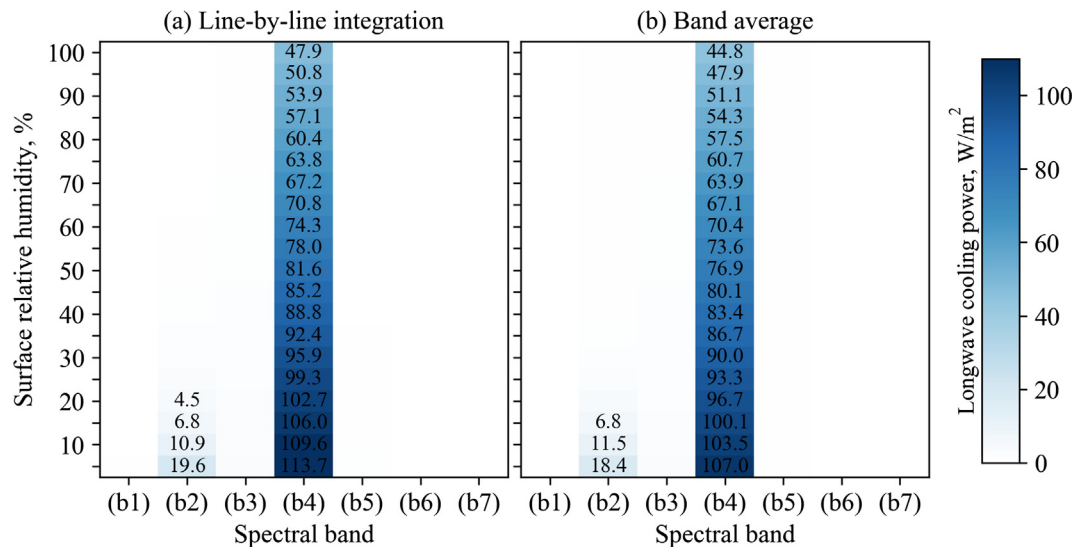


**Fig. 11.** Longwave cooling power by bands under clear skies for different ambient relative humidity with  $T_a = 294.2$  K. (a) line-by-line integration of  $q_{cool,lw}(v; T_a)$  for each band; (b)  $\varepsilon_{sky,j}$  per band calculated using the coefficients proposed in Table 2 with band-averaged emissivities for the passive cooler. Only values greater than  $4.0 \text{ W m}^{-2}$  are shown in the figure. The differences in values between (a) and (b) are smaller than 6%.

## Conflict of interest

The authors declared that there is no conflict of interest.

## Acknowledgments

The authors gratefully acknowledge partial support by the Department of Energy (DOE) Solar Energy Technology Office (SETO) project SFII#1649-1540, which is managed by Dr. Tassos Golnas.

## References

- [1] S. Buehler, A. Von Engeln, E. Brocard, V.O. John, T. Kuhn, P. Eriksson, Recent developments in the line-by-line modeling of outgoing longwave radiation, *J. Quant. Spectrosc. Radiat. Transf.* 98 (3) (2006) 446–457.
- [2] L. Zhou, R.E. Dickinson, Y. Tian, R.S. Vose, Y. Dai, Impact of vegetation removal and soil aridation on diurnal temperature range in a semiarid region: application to the Sahel, *Proc. Nat. Acad. Sci.* 104 (46) (2007) 17937–17942.
- [3] A. Donohoe, K.C. Armour, A.G. Pendergrass, D.S. Battisti, Shortwave and longwave radiative contributions to global warming under increasing  $\text{CO}_2$ , *Proc. Nat. Acad. Sci.* 111 (47) (2014) 16700–16705.
- [4] M. Brewster, Evaporation and condensation of water mist/cloud droplets with thermal radiation, *Int. J. Heat Mass Transf.* 88 (2015) 695–712.
- [5] B. Landro, P. McCormick, Effect of surface characteristics and atmospheric conditions on radiative heat loss to a clear sky, *Int. J. Heat Mass Transf.* 23 (5) (1980) 613–620.
- [6] P. Berdahl, M. Martin, F. Sakka, Thermal performance of radiative cooling panels, *Int. J. Heat Mass Transf.* 26 (6) (1983) 871–880.
- [7] M. Shen, S. Piao, S.-J. Jeong, L. Zhou, Z. Zeng, P. Ciais, D. Chen, M. Huang, C.-S. Jin, L.Z. Li, et al., Evaporative cooling over the Tibetan Plateau induced by vegetation growth, *Proc. Nat. Acad. Sci.* 112 (30) (2015) 9299–9304.
- [8] M. Li, Y. Jiang, C.F.M. Coimbra, On the determination of atmospheric longwave irradiance under all-sky conditions, *Sol. Energy* 144 (2017) 40–48.
- [9] L. Zhu, A.P. Raman, S. Fan, Radiative cooling of solar absorbers using a visibly transparent photonic crystal thermal blackbody, *Proc. Nat. Acad. Sci.* 112 (40) (2015) 12282–12287.
- [10] A.P. Raman, M.A. Anoma, L. Zhu, E. Rephaeli, S. Fan, Passive radiative cooling below ambient air temperature under direct sunlight, *Nature* 515 (7528) (2014) 540.
- [11] Z. Chen, L. Zhu, A. Raman, S. Fan, Radiative cooling to deep sub-freezing temperatures through a 24-h day-night cycle, *Nat. Commun.* 7 (2016) 13729.
- [12] Y. Zhai, Y. Ma, S.N. David, D. Zhao, R. Lou, G. Tan, R. Yang, X. Yin, Scalable-manufactured randomized glass-polymer hybrid metamaterial for daytime radiative cooling, *Science* 355 (6329) (2017) 1062–1066.
- [13] Z. Huang, X. Ruan, Nanoparticle embedded double-layer coating for daytime radiative cooling, *Int. J. Heat Mass Transf.* 104 (2017) 890–896.
- [14] M. Li, Z. Liao, C.F.M. Coimbra, Spectral model for clear sky atmospheric longwave radiation, *J. Quant. Spectrosc. Radiat. Transf.* 209 (2018) 196–211.
- [15] G.P. Anderson, S.A. Clough, F.X. Kneizys, J.H. Chetwynd, E.P. Shettle, AFGL atmospheric constituent profiles (0.120 km), Tech. rep., DTIC Document, 1986.
- [16] I.B. Pollack, T.B. Ryerson, M. Trainer, J. Neuman, J.M. Roberts, D.D. Parrish, Trends in ozone, its precursors, and related secondary oxidation products in Los Angeles, California: a synthesis of measurements from 1960 to 2010, *J. Geophys. Res.: Atmos.* 118 (11) (2013) 5893–5911.
- [17] I.E. Gordon, L.S. Rothman, C. Hill, R.V. Kochanov, Y. Tan, P.F. Bernath, M. Birk, V. Boudon, A. Campargue, K. Chance, et al., The HITRAN2016 molecular spectroscopic database, *J. Quant. Spectrosc. Radiat. Transf.* 203 (2017) 3–69.
- [18] E.J. Mlawer, V.H. Payne, J.-L. Moncet, J.S. Delamere, M.J. Alvarado, D.C. Tobin, Development and recent evaluation of the MT\_CKD model of continuum absorption, *Philos. Trans. Roy. Soc. Lond. Math. Phys. Eng. Sci.* 370 (2012) 2520–2556.
- [19] G.W. Petty, *A First Course in Atmospheric Radiation*, Sundog Publishing, Madison, WI, 2006.
- [20] M. Lee, Scaling anisotropic scattering in radiation heat transfer for a planar medium, *Urbana 2* (1982) 61801.
- [21] C.F.M. Coimbra, M. Li, Z. Liao, Efficient model for evaluation of spectral and vertical distributions of atmospheric longwave radiation, *International Heat Transfer Conference*, vol. 16, Begell House, 2018, <https://doi.org/10.1615/ihtc16.rti.023041>.
- [22] D.K. Edwards, The plating algorithm for radiation script-F transfer factor, *ASME J. Heat Transf.* 108 (1) (1986) 237–238.
- [23] D. Brunt, Notes on radiation in the atmosphere, *Quart. J. Roy. Meteorol. Soc.* 58 (247) (1932) 389–420.